Available online at www.sciencedirect.com

SciVerse ScienceDirect

Journal of the European Ceramic Society 32 (2012) 1857–1866

www.elsevier.com/locate/jeurceramsoc

Processing route dramatically influencing the nanostructure of carbon-rich SiCN and SiBCN polymer-derived ceramics. Part I: Low temperature thermal transformation

Yan Gao [a], Gabriela Mera [a,*], Hong Nguyen [a], Koji Morita [a,b], Hans-Joachim Kleebe [c], Ralf Riedel [a]

[a] *Technische Universität Darmstadt, Fachbereich Material- und Geowissenschaften, Petersenstrasse 23, Darmstadt D-64287, Germany*
[b] *National Institute for Materials Science, Materials Engineering Laboratory, Tsukuba, Ibaraki, Japan*
[c] *Technische Universität Darmstadt, Institut für Angewandte Geowissenschaften, Schnittspahnstraße 9, D-64287 Darmstadt, Germany*

Available online 5 October 2011

Abstract

In this study, the significant effect of the processing route on the nanostructure evaluation of carbon-rich SiCN and SiBCN polymer-derived ceramics is reported. For the first time, bulk carbon-rich SiCN and SiBCN ceramics are successfully produced by warm pressing of polyphenylvinylsilylcarbodiimide and polyborophenylsilylcarbodiimide. The bulk samples were compared with their analogous powder samples with respect to the developed nanostructure. Representative temperatures of 1100 and 1400 °C were chosen in order to investigate the effect of processing route used on the crystallization behavior of those samples. As the solid-state structure of polymer-derived ceramics (PDCs) is highly sensitive to the molecular structure of the precursor, the variation of processing route and pyrolysis temperature during the polymer to ceramic transformation and decomposition enables to alter the nanostructure of PDCs. It was found that the bulk carbon-rich SiCN and SiBCN ceramics show an improved thermal stability against crystallization as compared to their powder analogues.

Keywords: Precursor-organic; Electron microscopy; Microstructure; Processing; Carbon-rich polymer-derived SiCN and SiBCN ceramic

1. Introduction

Due to their strong dependence on the preceramic polymer chemistry, ceramic nanostructure and properties, polymer-derived ceramics (PDCs) have gained a lot of attention in recent years.[1–4] The thermal transformation of the polymers to ceramics is an emerging chemical process as attested by the increasingly commercial development of preceramic polymers.[1–3] The resulting ceramics are defined as intrinsically complex nanostructured systems which undertake several microstructural changes when exposed to temperatures higher than 1000 °C.[1–5] PDCs are X-ray amorphous but nanoscopically heterogeneous materials obtained by the thermal decomposition of organic polymers providing ternary and quaternary ceramics, impossible to be obtained by classical powder synthesis. Polymer-derived ternary and multinary ceramics based on SiCN and SiBCN systems are refractory materials processing resistance to crystallization and creep deformation to high temperatures[1–3] which are improved when the ceramics are fabricated with a high content of free carbon.[6]

There is a strong relationship between the chemistry, processing route and the final nanostructure of polymer-derived ceramics. Therefore, the properties of PDCs and their potential applications depend as well to a great extent on the chemistry of the precursors and their processing route.

One main feature of polymer-derived ceramics is their possibility to incorporate an extremely high content of free carbon into the microstructure. Studies on carbon-rich SiCN,[6–8] as well as SiCO[9–12] systems shown that these ceramics have a much higher stability against crystallization than the low carbon containing analogues, the carbon-rich ceramics remaining amorphous up to higher temperatures, when the finely dispersed free carbon phase is acting as a diffusion barrier. Therefore, a key question in understanding the transformation of the polymeric state to a nanostructured ceramic is the role played by the free carbon, going from ceramics in form of powders to bulk materials.

The well-known precursors for silicon carbonitride (SiCN) ceramics are the polysilazanes $–[R^1R^2Si–NR^3]_n–$ and the

* Corresponding author. Tel.: +49 (0)6151 166340; fax: +49 (0)6151 166346.
E-mail address: mera@materials.tu-darmstadt.de (G. Mera).

0955-2219/$ – see front matter © 2011 Elsevier Ltd. All rights reserved.
doi:10.1016/j.jeurceramsoc.2011.09.012

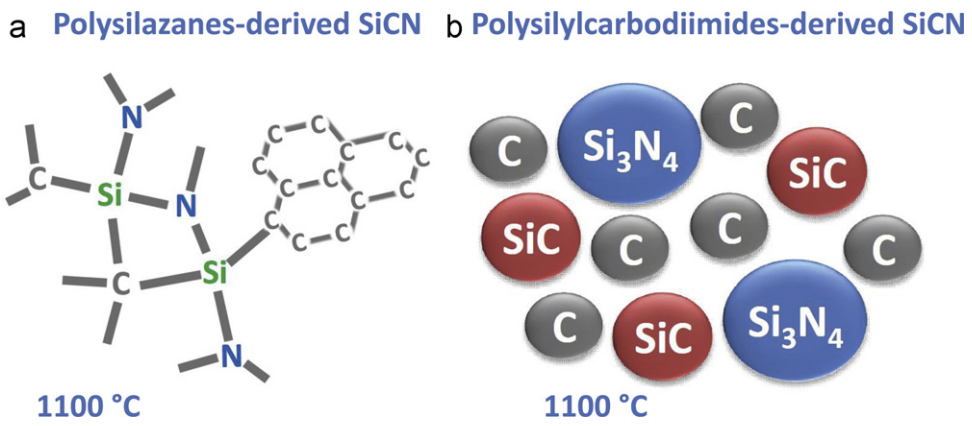

Fig. 1. Role of the chemistry of the precursors on the microstructure of SiCN ceramics obtained from polysilazanes (left) and carbon-rich polysilylcarbodiimides (right) after the pyrolysis in argon at 1100 °C.[1–3,6,7]

polysilylcarbodiimides $–[R^1R^2Si–N{=}C{=}N]_n–$, where R^1, R^2 and R^3 are organic groups such as methyl, phenyl, etc. Differences between the microstructure of amorphous SiCN ceramics obtained from polysilazanes and polysilylcarbodiimides are presented in Fig. 1. By the thermal decomposition of polysilazanes $–[R^1R^2Si–NR^3]_n–$, as demonstrated by solid-state NMR studies,[1–3] a single phase amorphous structure can be obtained (Fig. 1a). In this case, silicon is bonded to nitrogen and carbon at the same time. Moreover, segregation of large domains of free carbon was also observed. The thermal decomposition of polysilylcarbodiimides was characterized by solid-state NMR and SAXS spectroscopy.[6,7] Contrary to the case of the SiCN ceramics obtained from polysilazanes, the pyrolysis of polysilylcarbodiimides $–[R^1R^2Si–N{=}C{=}N]_n–$ yields a mixture of several amorphous phases depending on the amount of the free carbon phase.[6,7] The microstructure of low-carbon containing polysilylcarbodiimides are characterized by the presence of two amorphous phases, namely amorphous Si_3N_4 (a-Si_3N_4) and amorphous carbon (a-C). As recently demonstrated, the pyrolysis of carbon-rich polysilylcarbodiimides[6,7] provides a microstructure composed of three amorphous phases, a-Si_3N_4, a-SiC and a-C as presented in Fig. 1b.

The presence of "free" carbon and also of additional elements such as boron is dramatically influencing the properties of the ceramics with respect to their microstructure. Structural disorder in carbon-rich SiBCN ceramics, which results in increased free activation energies of both crystallization and solid-state reaction of the Si–N bond with carbon, is considered to be responsible for the thermal stability of these materials. Carbon-rich polymer-derived silicon boron carbonitride materials (SiBCN) are defined as complex nanostructured systems which have remarkably higher thermal, chemical and mechanical (creep) stability than boron-free counterparts even at temperatures up to 2000–2200 °C in inert atmosphere.[13,14]

The polymer-derived ceramic route is also an efficient and promising method in order to produce complex-shaped bulk ceramics using the advantages of plastic technologies.[1–3] However, pyrolysis of precursors is always accompanied by the evolution of gaseous byproducts and by the significant shrinkage, which it can introduce pores, stresses, deformation. A lot of efforts were made in order to get dense bulk ceramics[15–27] and among them the uniaxial warm press technique is one of the most frequently used processes. However, no results about the processing of bulk SiCN ceramics obtained from polysilylcarbodiimides were reported yet.

In this publication we report for the first time on the nanostructure characterization of carbon-rich SiCN and SiBCN polymer-derived ceramics depending on their processing route, namely as ceramic powders or bulk ceramics. No synthesis and TEM characterization of bulk carbon-rich SiCN and SiBCN ceramics derived from polysilylcarbodiimides and respectively, polyborosilylcarbodiimides have been published yet. In this paper, the characterization of the carbon-rich polymer-derived ceramics was accomplished by elemental analysis, SEM and the local analysis made by HRTEM microscopy. The final microstructure is discussed with respect to the precursor chemistry, processing route (powder and bulk synthesis), temperature, presence of boron and "free" carbon content. The results emphasize the strong relationship between chemistry ↔ processing ↔ nanostructure of carbon-rich SiCN and SiBCN ceramics.

2. Materials and methods

2.1. Chemicals

Phenylvinyldiphenylsilane, borane dimethylsulphide and pyridine were purchased from Sigma–Aldrich Chemie GmbH, Germany. All chemicals were used as received without further purification. Bis(trimethylsilyl)carbodiimide was synthesized according to the literature.[28]

2.2. Synthesis and pyrolysis

All reactions were carried out in purified argon atmosphere using standard Schlenk techniques.[29] Polyphenylvinylsilylcarbodiimide (HN1) was synthesized as recently reported[6] starting from bis(trimethylsilyl)carbodiimide and phenylvinyldichlorosilane in the presence of pyridine as catalyst. Polyborophenylvinylsilylcarbodiimide (HN1B) was obtained

from hydroboration of polyphenylvinylsilylcarbodiimide (HN1) in toluene as solvent at 0 °C.

The ceramics at 1100 and 1400 °C were obtained in form of powders and bulk ceramics. For the powder ceramic pyrolysis up to 1100 °C, 3–5 g of precursor were filled in a quartz crucible, put in a quartz tube and closed under argon atmosphere. The tube was placed in programmable horizontal tube-furnace and heated under a steady flow of purified argon. The samples were pyrolyzed as follows: heating up to 1100 °C with 100 °C h^{-1}, then 2 h dwelling time at 1100 °C, followed by cooling down to room temperature. The bulk ceramics were synthesized using a uniaxial warm-press process in order to crosslink and shape the polymers, followed by the pyrolysis of the green bodies in the same way as the powder ceramics. The polyphenylvinylsilylcarbodiimide is a honey-like polymer; therefore a precrosslinking of the sample at 255 °C for 5 h was used before warm pressing. In this way, a powder-like soluble precrosslinked polymer HN1 was obtained. The presence of vinyl-groups in the precrosslinked polymer was proved by means of liquid-state NMR and FTIR spectroscopy. In the case of polyborophenylsilylcarbodiimide HN1B, no precrosslinking was necessary due to the powder-like physical properties of the polymer after hydroboration.

The warm pressing of precrosslinked HN1 and HN1B polymers was performed using uniaxial warm press machine (die diameter 10 mm). The parameters used for the warm-pressing were as follows: for HN1 precrosslinked material temperature 200 °C, pressure 26 MPa, holding time 2 h; for HN1B polymer temperature 220 °C, pressure 88 MPa, holding time 2 h. In both cases, compact and mechanically stable green bodies were produced.

The post-annealing experiments at 1400 °C were performed in an Astro furnace, Thermal Technology Inc., CA, USA in argon atmosphere. The powders, respectively the bulk ceramics obtained at 1100 °C were placed in a silicon carbide crucible and pyrolyzed with a heating ramp of 5 °C/min to the 1400 °C and kept for 2 h. The thermolysis was completed by cooling the samples to room temperature with a cooling ramp of 10 °C/min.

2.3. Characterization techniques

All micro-Raman spectra (excepting the bulk samples at 1400 °C) (10 scans, each lasting 3 s) were recorded with a Horiba HR800 micro-Raman spectrometer (Horiba Jobin Yvon, Bensheim, Germany) equipped with an Ar laser (irradiation wavelength 514.5 nm). The excitation line has its own interference filter (to filter out the plasma emission) and a Raman notch filter (for laser light rejection). The measurements were performed with a grating of 1800 g mm^{-1} and a confocal microscope (magnification 50×, NA 0.5) with a 100 μm aperture, giving a resolution of 2–4 μm. The laser power (ca. 20 mW) on the sample was attenuated in the range of 2 mW–20 μW using neutral density (ND) filters. For samples HN1 1400 °C bulk and HN1B 1400 °C bulk, the Raman spectroscopy was measured also with excitation wavelength of 514.5 nm (tunable Ar+ Laser, Melles Griot, Albuquerque, NM) in a 180° backscattering geometry on Holospec VPH spectrometer (Kaiser Optical Systems, Ann Arbor, MI). For the evaluation of free carbon cluster size in ceramics, Gaussian curve fitting of the Raman bands (OriginPro 8.1 Software) was applied. All-reflecting objective (ARO) IR micro-spectroscopy was done on a confocal IlluminatIR™ FTIR spectrometer (Horiba Jobin Yvon, Bensheim, Germany) using reflection absorption spectroscopy (RAS) for quick analysis. The spectrum of the microscopic specimen is recorded by simply focusing on the specimen.

Scanning electron microscopy (SEM) micrographs were obtained using an FEI Quanta 600 instrument (FEI, Eindhoven, The Netherlands). The samples were sputtered with a conductive gold layer prior to investigation.

For the chemical composition analysis, the carbon content of the samples was determined with a carbon analyzer, CS 800 (Eltra GmbH, Neuss) and the oxygen and nitrogen content with a N/O analyzer, Leco TC-436 (Leco Corporation, Michigan). Hydrogen, boron and chlorine chemical composition of the ceramics at 1100 °C were carried out at Mikroanalytisches Labor Pascher (Remagen, Germany). The silicon fraction was calculated as the difference between 100% and the values of the other elements.

Transmission electron microscopy (TEM) of the powder ceramics was performed using an FEI CM20STEM instrument (FEI, Eindhoven, The Netherlands) operating at an acceleration voltage of 200 kV (wavelength $\lambda = 2.51$ pm). For the TEM sample preparation, the ceramic powders were dispersed in an ultrasonic bath (high purity methanol 99.8%, Sigma–Aldrich Co.) and a small droplet of the suspension was placed on holey carbon (Cu) grit. Upon drying, the samples were lightly coated with carbon to avoid charging under the electron beam. TEM samples of the bulk materials were prepared via conventional preparation techniques involving cutting, grinding and polishing, followed by Ar-ion milling and light carbon coating. The same instrument, FEI CM20STEM, utilized for the powder characterization was used for the study of the bulk samples.

3. Results and discussion

The synthesis and processing of the polyphenylvinylsilylcarbodiimide HN1 and polyborophenylsilylcarbodiimide HN1B were done as described in the experimental part and summarized in Fig. 2. The synthesis of polyphenylvinylsilylcarbodiimide was carried out as previously reported[6] and therefore not presented in Fig. 2.

In order to shape the polyphenylvinylsilylcarbodiimide HN1 polymer by means of warm-pressing, a precrosslinking process was necessary. The liquid polymer HN1 (Fig. 2) was precrosslinked at 255 °C for 5 h in order to get a yellow powder which still contains reactive vinyl groups necessary for the final crosslinking and shaping in the warm press (Fig. 3).

In order to understand the influence of the chemistry of the precursors, as well as the processing route on the final nanostructure of the ceramics, two temperatures of pyrolysis have been chosen. First, 1100 °C was selected as standard temperature for amorphous PDCs and 1400 °C, as temperature when the nanostructure and the crystallization trend is strongly depending on the composition and architecture of starting precursors.

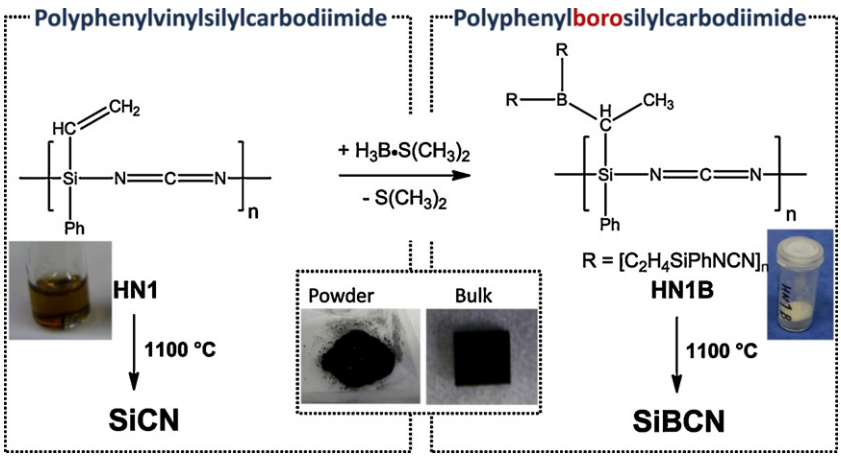

Fig. 2. Synthesis and processing of polyphenylvinylsilylcarbodiimide HN1 and polyborophenylsilylcarbodiimide HN1B.

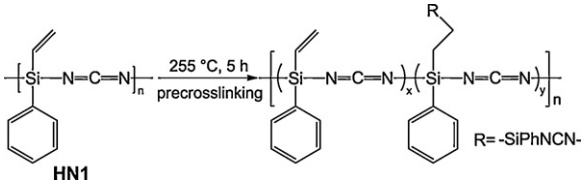

Fig. 3. Precrosslinking reaction of polyphenylvinylsilylcarbodiimide HN1.

The microstructure of the green bodies and of the pyrolyzed bulk ceramics were observed and studied by SEM. A SiCN(O) surface layer, in which some cracks and pores exist, was found on the surface of bulk ceramics HN1 and HN1B 1100 °C. Fig. 4 shows the presence of this layer of ~3 μm thick in the case of HN1 1100 °C sample. Under the SiCN(O) layer, the ceramic is very dense, showing no defects. The same microstructural characteristics were found also in the case of SiBCN ceramic HN1B 1100 °C. The formation of the SiCN(O) layer is due to the removal of the green body in air after the warm pressing process. In order to avoid the influence of formation of SiCN(O) layer on the microstructure of bulk ceramics, the 1100 °C samples were polished before annealing at 1400 °C.

FTIR is an important integral method for the characterization of the bonding situation and respectively, the microstructure of the ceramics. Fig. 5 presents the ARO FTIR (all-reflecting objective FTIR) of HN1 polymer derived SiCN and SiBCN bulk and powder samples.

As shown by FTIR, the majority of the bands are corresponding to the free carbon phase (1652, 1583, 1503, 1447, 1378 cm^{-1}). All ceramics still contain C(sp^3)–H bands (C–H asymmetric and symmetric stretching vibrations at 2924 and 2860 cm^{-1}) probably as terminally saturated groups in the graphene-like carbon phase. The most important bands are related to the presence of Si_3N_4 and SiC phases (Si–N stretching vibration at 970 cm^{-1} and Si–C stretching at 812 cm^{-1}). Remarkably, the FTIR of all samples contains also C=N (stretching vibration at 1720 cm^{-1}) and C–N (stretching at 1253 and 1188 cm^{-1}). Moreover, the FTIR spectrum of HN1 1400 °C powder shows a highly intensive band for Si–C due to the crystallization of SiC (812 cm^{-1}). The intensity of Si_3N_4 band is also varied depending on temperature and processing route. For bulk ceramics, the silicon nitride band is strong, independently on the temperature of annealing. In the case of powder ceramics, at 1400 °C the Si–N band is less intensive as in the case of 1100 °C analogue. This observation is matching very well with the increase in the intensity of SiC band. The ceramics are losing nitrogen by the carbothermal reaction of Si_3N_4 with carbon to form SiC and nitrogen gas: a-Si_3N_4 + 3 a-C → 3 α/β-SiC + $2N_2$ ↑

Raman spectroscopy is the key nondestructive tool for the examination of the structural evolution of the free carbon phase in PDCs.[30–34] The representative features of free carbon in the Raman spectra of PDCs are the so-called disorder-induced D-band at approx. 1350 cm^{-1} and the G band at approx. 1582 cm^{-1} due to in-plane bond stretching of sp^2 carbon, as well as the

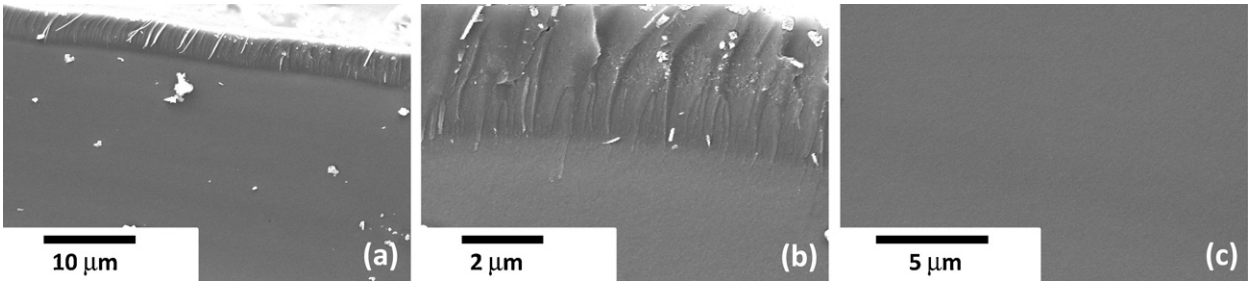

Fig. 4. SiCN HN1 1100 °C cross-section: (a) and (b) thin SiCN(O) layer on the surface; (c) defect-free bulk SiCN ceramic under the SiCN(O) layer.

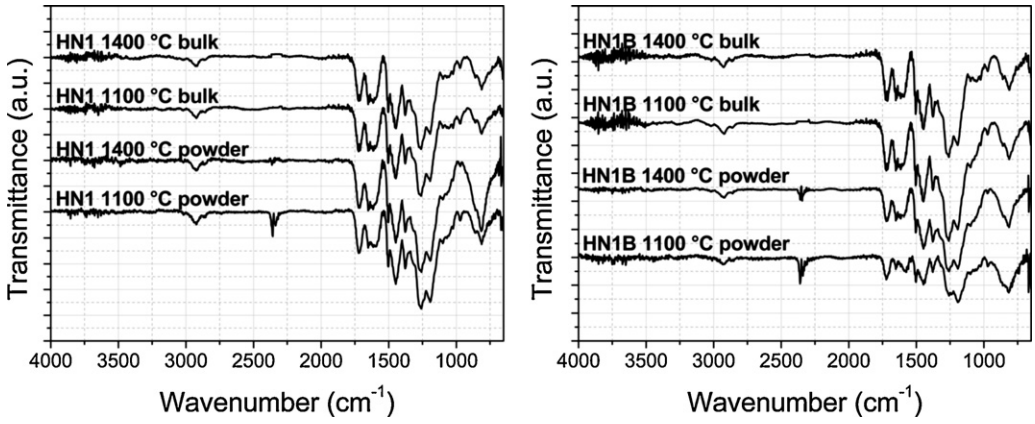

Fig. 5. ARO FTIR spectroscopy of (a) SiCN ceramics and (b) SiBCN ceramics at 1100 and 1400 °C.

G′-band (the overtone of the D-band which is always observed in defect-free samples at 2700 cm^{-1}).[30–34] The D and G bands can vary in intensity, position and width, depending on the structural organization of the sample under investigation. The intensity ratio of the D and G modes, I_D/I_G, enables the evaluation of the carbon-cluster size by using the formula reported by Ferrari and Robertson[30]:

$$\frac{I_D}{I_G} = C'(\lambda)L_a^2$$

where, L_a is the size of carbon domains along the six fold ring plane (lateral size), and C' is a coefficient that depends on the excitation wavelength of the laser. The value of the coefficient C' for the wavelength of 514.5 nm of the Ar-ion laser employed here is 0.0055 $Å^{-2}$. Gaussian curve fitting of the Raman bands was performed in order to extract the I_D/I_G intensity ratios and to determine the size of the free carbon cluster formed in the ceramics. The peak fitting was done including the minor bands T (shoulder at ∼1200 cm^{-1}), attributed to sp^2–sp^3 C–C and C=C bonds presence and D″ at ∼1500 cm^{-1} corresponding to the fraction of amorphous carbon contained in the samples.[35] The reason for these additional bands is that the structural disorder can activate otherwise forbidden vibration modes[36,37] (see Fig. 6).

The micro-Raman spectra of all samples are characterized by broad and overlapped D and G bands indicating a strong disorder state. The disorder in the carbon phase can be primary induced by the presence of edges in the graphene layers, by the deviation from planarity of graphene layers and also by the presence of carbon atoms in sp^3 hybridization state. Recently, the dependence of I_D/I_G ratio on the degree of disorder in graphene-like materials was reported.[38–40] The disorder was quantified as depending on point-like defects. Assuming that we have a low defect density, the typical interdefect distance L_D can be calculated with the formula: $I_D/I_G = C(\lambda)/L_D^2$, valid when $L_D > 6$ nm (C (514.5 nm) ≈ 107 nm^2).[38–40] Unfortunately, the equation is not valid for high defect density but even though, it can help to compare the samples prepared with different processing routes. The processing of ceramics as bulk is expected to decrease the density of defects in the carbon phase. The interdefect distances L_D together with the ratio of D and G and lateral cluster size L_a are summarized in Table 1. Excepting the sample HN1B 1100 °C powder, all other ceramics show valid L_D distances calculated as reported before. For the HN1B 1100 °C powder sample, the distance between defects (L_D = 5.71 nm) is lower than the limit of validity of the equation ($L_D > 6$ nm), and therefore omitted from discussion. As observed in Table 1, the bulk samples show less density of defects than the powder samples. Moreover, at 1400 °C the carbon phase is more organized than at 1100 °C and also shows less defects. Moreover, the presence of boron decreases the density of defects and enhances the organization of the carbon. Especially at 1100 °C, the HN1B bulk shows a decrease in the lateral size of carbon (1.41 nm) and on the ratio I_D/I_G due a highly organization of the graphene layers. This fact is underlined also by the presence of a sharp single Gaussian peak for G′ band at 2672.62 cm^{-1}. Regarding the lateral size of the carbon clusters in the SiCN ceramics, a decrease is observed when comparing the 1400 °C sample with the one at 1100 °C, trend observed in both cases, of powder and bulk ceramics.

Table 1
The Raman parameters of the free carbon phase in powder and bulk SiCN and SiBCN ceramics.

Sample	I_D/I_G	L_a (nm)	L_D (nm)
HN1 1100 °C powder	2.61	2.18	6.40
HN1 1400 °C powder	1.71	1.76	7.91
HN1 1100 °C bulk	2.54	2.15	6.49
HN1 1400 °C bulk	1.92	1.87	7.47
HN1B 1100 °C powder	3.28	2.44	5.71
HN1B 1400 °C powder	2.43	2.10	6.64
HN1B 1100 °C bulk	1.09	1.41	9.90
HN1B 1400 °C bulk	2.61	2.18	6.40

The composition of SiCN and SiBCN ceramics was determined by means of elemental analysis for the powder and bulk samples (Table 2).

Regarding the composition of the powder samples compared to their bulk analogues, it was observed that the powder ceramics at 1100 °C and 1400 °C contain a higher content of carbon and nitrogen. In the same time, the silicon content is higher in the bulk ceramics. Another interesting observation is that the content of hydrogen and chlorine registered in the powder ceramics at 1100 °C is not present anymore in the bulk

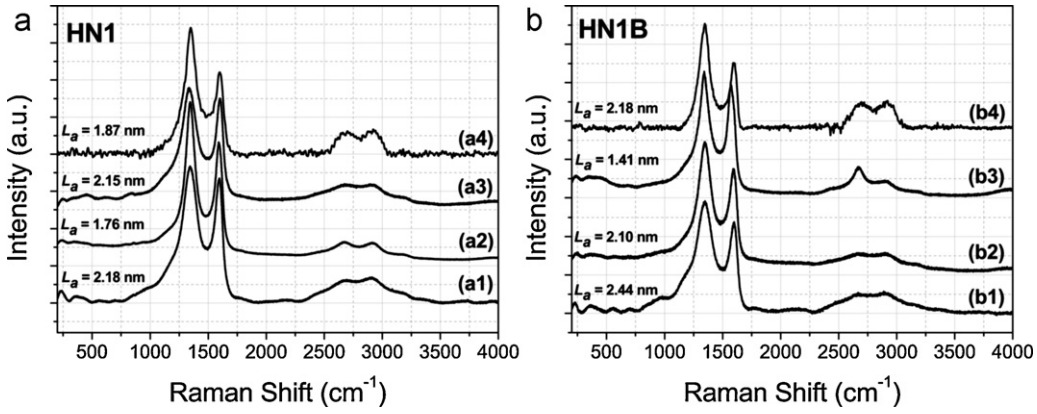

Fig. 6. Micro-Raman spectroscopy of (a) SiCN ceramics (a1) HN1 1100 °C powder; (a2) HN1 1400 °C powder; (a3) HN1 1100 °C bulk; (a4) HN1 1400 °C bulk; and (b) SiBCN ceramics: (b1) HN1B 1100 °C powder; (b2) HN1B 1400 °C powder; (b3) HN1B 1100 °C bulk; (b4) HN1B 1400 °C bulk. The corresponding cluster size of carbon (L_a) for each measurement is provided in the graphs.

ceramics at the same temperature. Even if FTIR study is showing the presence of C–H bonds in bulk ceramics, the amount of hydrogen is less than the limit of detection for elemental analysis. The differences in the Si, C, N, H and Cl composition should be attributed to the changes in the chemistry and architecture of precursors using different routes of processing. The processing of bulk ceramics includes a crosslinking and shaping step which allows the formation of a 3D structure and the elimination of the end-group chlorine from the precursor. Boron content in all SiBCN samples is constant, no variation being register between bulk and powder ceramics. As presented in Fig. 4, the bulk HN1 and HN1B at 1100 °C show a SiCN(O) 3 μm thick layer on the surface. In order to understand how the presence of this layer can change the composition of the samples, the elemental analysis was done without polishing it. As expected, the HN1 1100 °C bulk and HN1B 1100 °C bulk contain a high amount of oxygen contamination of 9.15, respectively 11.84%. The 1400 °C analogues were prepared after polishing the oxygen-containing layer, showing, as expected, less oxygen contamination.

High-resolution TEM microscopy (HRTEM) is a powerful method in order to locally investigate the nanostructure evolution of polymer-derived ceramics at different temperatures of annealing. Even if the PDCs are X-ray amorphous at low temperatures ($T < 1400$ °C), they are typically heterogeneous as shown by several TEM studies.[41–43] Until now, there is a lack of information regarding the TEM investigations of polysilylcarbodiimides-derived ceramics. Due to the complicated and so far impossible processing of these precursors as bulk monoliths, no nanostructure investigation of these ceramics was reported. This study presents an easy route to bulk carbon-rich polysilylcarbodiimides-derived ceramics and their nanostructure analysis by means of TEM. The comparison between bulk and powder SiCN ceramics is underlining the importance of crosslinking and shaping processes on the thermal stability of PDCs. Moreover, the effect of a low amount of boron in these materials is commented with respect to the nanostructure characteristics.

Fig. 7 presents the bulk SiCN and SiBCN ceramics at 1100 °C. The selected area electron diffraction (SAED) of the SiCN and SiBCN ceramics at 1100 °C is displayed as inset in this figure. All four ceramics, independently on composition or processing route show a diffuse elastically scattered ring pattern, typical for amorphous samples. No major contrast variation was observed for the samples annealed at 1100 °C, indicating the amorphous nature of all samples. Even at higher magnification, no indication of any crystalline phase could be imaged. At this low temperature of pyrolysis, no difference can be observed between the nanostructure of powder and bulk SiCN ceramics with or without boron.

In the case of powder SiCN and SiBCN ceramics pyrolyzed at 1400 °C, high-resolution TEM imaging shows that the ceramics

Table 2
Chemical composition of the powder and bulk SiCN and SiBCN ceramics.

Sample	Chemical composition							Empirical formula
	Si %	C %	N %	B %	O %	H %	Cl %	
HN1 1100 °C powder	24.80	56.50	14.80	–	2.14	0.24	1.55	$SiC_{5.32}N_{1.19}H_{0.27}Cl_{0.05}O_{0.15}$
HN1 1100 °C bulk	28.45	51.42	10.98	–	9.15	–	–	$SiC_{4.22}N_{0.77}O_{0.56}$
HN1B 1100 °C powder	23.79	51.32	16.58	3.05	2.21	0.30	2.75	$SiB_{0.33}C_{5.04}N_{1.40}H_{0.35}Cl_{0.09}O_{0.16}$
HN1B 1100 °C bulk	28.81	42.31	13.63	3.41	11.84	–	–	$Si_1B_{0.30}C_{3.43}N_{0.88}O_{0.72}$
HN1 1400 °C powder	25.24	59.21	11.03	–	0.52	–	–	$SiC_{5.47}N_{0.87}O_{0.04}$
HN1 1400 °C bulk	28.65	57.06	11.66	–	2.63	–	–	$SiC_{4.65}N_{0.81}O_{0.16}$
HN1B 1400 °C powder	28.21	51.08	16.19	3.06	1.46	–	–	$SiB_{0.28}C_{4.23}N_{1.07}O_{0.09}$
HN1B 1400 °C bulk	29.15	48.62	14.62	3.45	4.16	–	–	$SiB_{0.30}C_{3.89}N_{0.94}O_{0.25}$

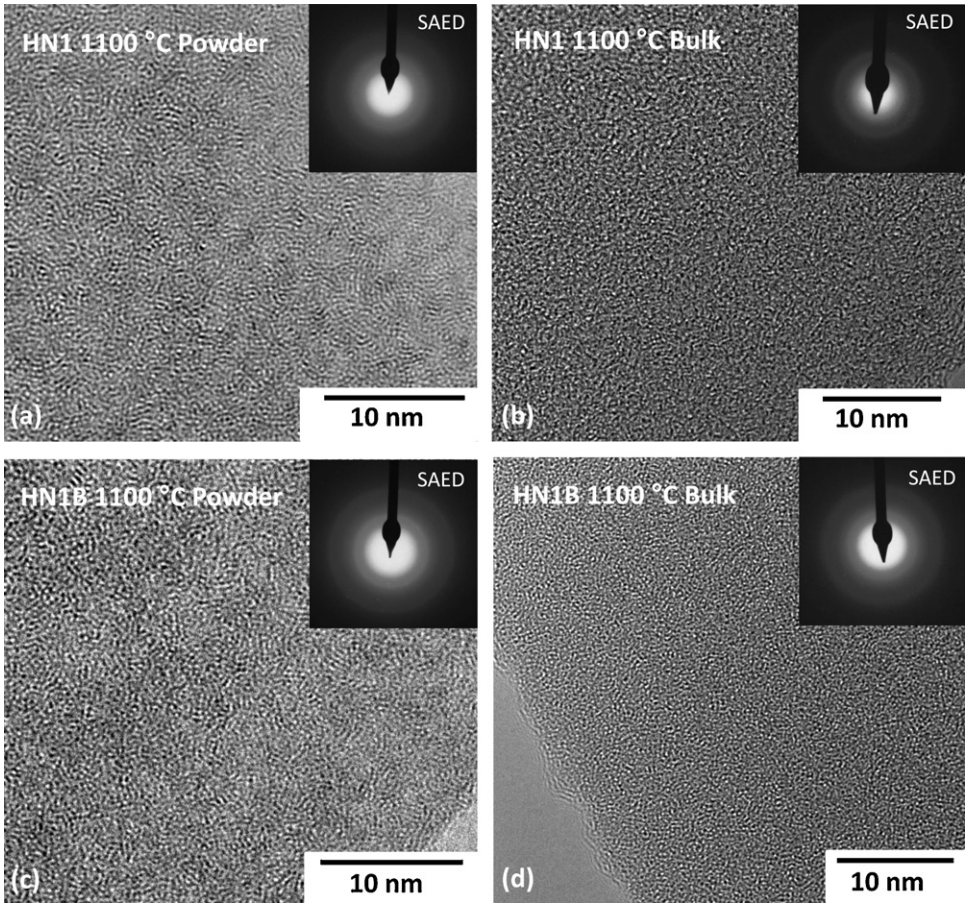

Fig. 7. HRTEM images of powder and bulk SiCN and SiBCN ceramics at 1100 °C (the insets present the selected area electron diffraction): (a) SiCN HN1 1100 °C powder; (b) SiCN HN1 1100 °C bulk; (c) SiBCN HN1B 1100 °C powder; (d) SiBCN HN1B 1100 °C bulk.

already started to crystallize. Fig. 8 displays the nanostructure characteristics of these ceramics where crystallites of α/β-SiC are embedded in a graphene-like carbon matrix. In addition, as indicated by the elemental analysis, in the amorphous matrix, amorphous Si_3N_4 is still present (Table 2). As previously reported for carbon-rich SiCN ceramics obtained from polysilylcarbodiimides, no crystallization of Si_3N_4 was recorded.[6] As observed in the SAED insets in Fig. 8, the SiBCN sample (Fig. 8b) shows an enhanced crystallization compared to the SiCN analogue. Thermodynamic modeling studies as well as experimental work proved that the presence of boron in SiCN ceramics is the driven force for SiC crystallization.[44–46] Indeed, also in the case of HN1B polyphenylborosilylcarbodiimide-derived SiBCN ceramic, the same enhancement of crystallization of SiC due to the presence of boron was observed.

In contrast to the nanostructure of SiCN and SiBCN powder ceramics, the investigation of the bulk analogues revealed *no* crystallization of α/β-SiC. Even at higher magnification, no

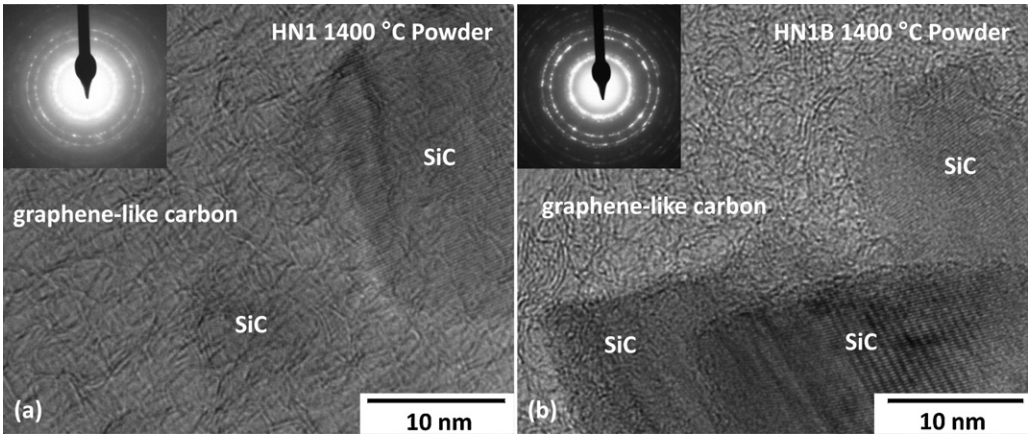

Fig. 8. HRTEM images of powder SiCN and SiBCN ceramics annealed at 1400 °C. The SAED patterns (insets) show the presence of α/β-SiC.

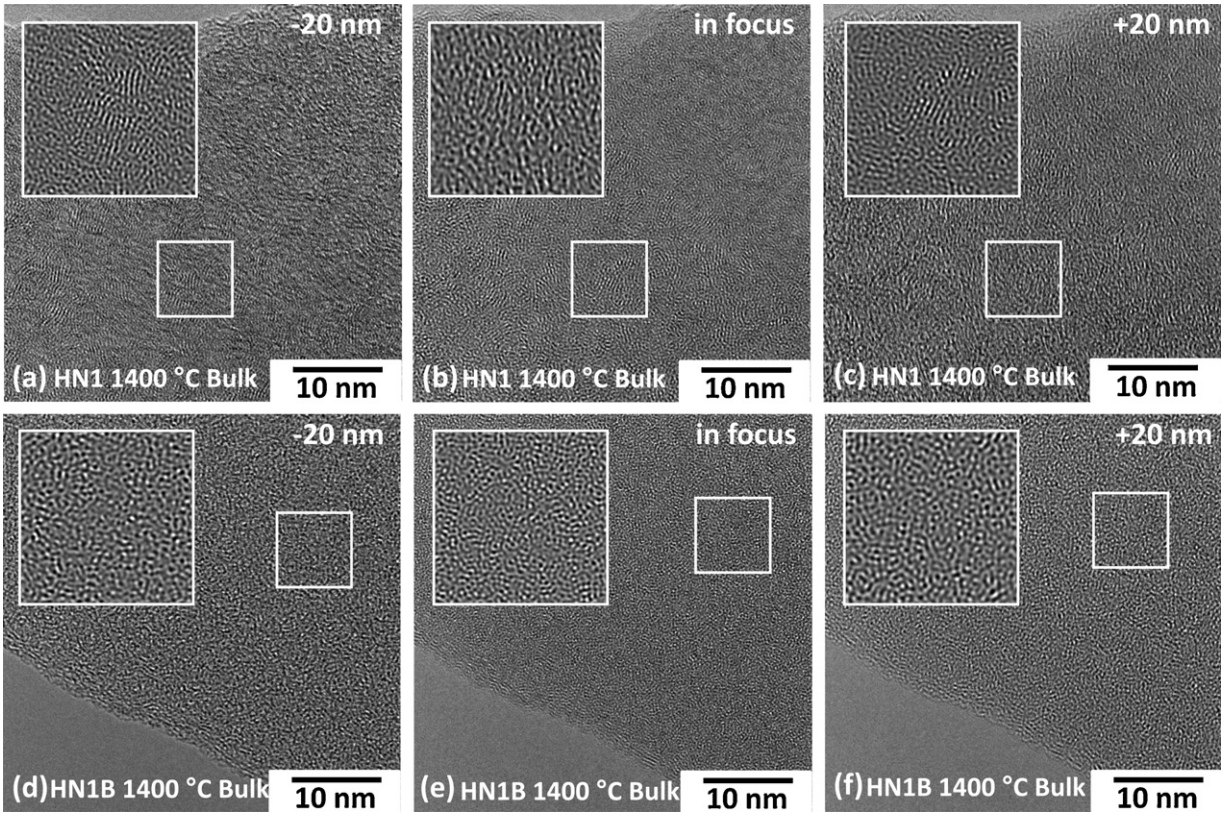

Fig. 9. HRTEM images of bulk SiCN and SiBCN ceramics pyrolyzed at 1400 °C. Different defocus setting of the objective lens were chosen since carbon and SiC can better be imaged at slight over- and underfocus conditions,[12] respectively; (a), (b), (c) SiCN 1400 °C bulk and (d), (e), (f) SiBCN 1400 °C bulk. The insets represent the inverse FFT images of the selected areas (boxed regions).

nucleation of SiC was observed. In order to assure the amorphous nature of the bulk samples, several TEM micrographs at different defocus setting of the objective lens were taken.

As reported in the case of polysilazanes-derived ceramics, with increasing temperature, the first crystallization event is the formation of basic structural units (BSU) of carbon, followed by the nucleation of SiC. Indeed, in the SiCN bulk ceramic annealed at 1400 °C, depending on the defocus setting of the objective lens, slight contrast variations are seen in the HRTEM image. At under-versus overfocus (−20 nm) (Fig. 9), see also the inverse fast Fourier transform (FFT) images, the defocus variation results in a slight change in the phase contrast, indicating a fine organization of the carbon phase. The FFT inset clearly shows the presence of a carbon phase (Fig. 10a), as also indicated in the inverse FFT image of a thicker region (Fig. 10b).

In the case of bulk SiBCN 1400 °C (Fig. 9d–f), depending on the defocus value of the objective lens, no phase contrast variations can be seen in the HRTEM image, the sample being fully amorphous. This fact can be due to the higher thermal stability of the SiBCN ceramic when it was assumed that the boron-containing carbon matrix, similar to graphene-like phase, acts as effective diffusion barrier preventing SiC nucleation. As presented in Table 2, the SiBCN ceramics, powder and bulk, contain only up to 3–3.4 wt% of boron, an amount which is obviously not enough to prevent SiC crystallization in the case of the higher surface area of the ceramic powder.

Differences in thermal stability against crystallization between powder samples and the bulk material are due to the surface nucleation and increased nanoporosity in the case of the powder ceramics. The enhancement of the specific surface area of powder-processed samples increases the “reactivity” of the materials, with regard to carbothermal reaction, and the materials start to crystallize at lower temperatures with higher rates. A similar trend was observed for different particle sizes of SiBCN ceramics investigated with respect to thermal decomposition and crystallization.[47] The skin-core effect reported for polyborosilazanes-derived ceramics[48] was not observed in our study.

It is already reported that in the case of SiBCN ceramics composed of Si_3N_4, SiC, BN and C, the thermal stability strongly depends on the boron content.[49,50] In our case, a low concentration of boron is expected to decrease the thermal stability of the ceramics against crystallization. However, at the same time, a high free carbon concentration is assumed to improve the thermal stability of these materials counterbalancing the boron effect.[14,51,52] As demonstrated by SAXS analysis for polysilylcarbodiimides-derived SiCN ceramics, the high excess free carbon causes the complexity of the nanostructure composed of small nanodomains of 1–3 nm in size. Smaller nanodomains are less susceptible to carbothermal reaction as the larger analogues. Furthermore, the surfaces provide active reaction sites for decomposition and crystallization.

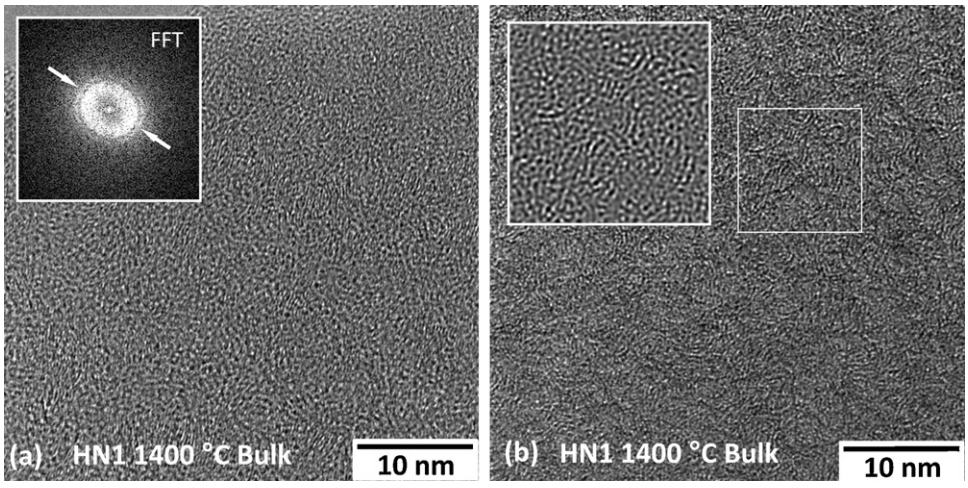

Fig. 10. (a) HRTEM micrographs of HN1 1400 °C bulk (the inset shows the FFT image corresponding to carbon phase); (b) inverse FFT image of the thick region of HN1 1400 °C bulk.

4. Conclusions

Polymer-derived SiCN and SiBCN ceramics were produced via a warm press process as bulk materials and by the simple thermal decomposition without crosslinking as powder materials. For the first time, dense defect-free bulk ceramics were obtained from polysilylcarbodiimides. The nanostructure investigations by means of high-resolution TEM show that the thermal stability of the ceramics strongly depends on the processing route and on the chemistry of the precursors (carbon content, precursor type and presence or absence of boron). The microstructure of SiCN and SiBCN powder ceramics at 1400 °C is characterized by the presence of α/β-SiC crystallites embedded in a matrix of amorphous carbon and Si_3N_4 in contrast to the bulk ceramics which remain completely amorphous at this temperature. Moreover, the presence of boron in the powder SiBCN ceramic promotes the crystallization of SiC. In the case of the bulk ceramics, the SiCN 1400 °C shows a finely organization of carbon.

In conclusion, in this paper was shown that the factors influencing the thermal stability against crystallization and decomposition are the chemical composition (in special the carbon content and presence of boron), the architecture of the polymer and the processing route which influences the residual porosity and surface area.

Acknowledgements

Financial support by the grants funded under the MWN (Materials World Network) of the DFG and the National Science Foundation as well as LOEWE-Zentrum AdRIA (Adaptronik—Research, Innovation, Application), funded by the state of Hesse, Germany and the Fonds der Chemischen Industrie, Frankfurt (Germany) is gratefully acknowledged. The authors thank Toni Groß for recording the Raman spectra of the bulk samples at 1400 °C.

References

1. Riedel R, Mera G, Hauser R, Klonczynski A. Silicon-based polymer-derived ceramics: synthesis properties and applications – a review. *J Ceram Soc Jpn* 2006;**114**:425–44.
2. Colombo P, Mera G, Riedel R, Soraru G-D. Polymer-derived ceramics: 40 years of research and innovation in advanced ceramics. *J Am Ceram Soc* 2010;**93**:1805–37.
3. Mera G, Riedel R. Organosilicon-based polymers as precursors for ceramics. In: Colombo P, Riedel R, Sorarù GD, Kleebe H-J, editors. *Polymer derived ceramics: from nanostructure to applications*. Lancaster, PA, USA: DEStech Publications Inc.; 2009. p. 51–89.
4. Papendorf B, Nonnenmacher K, Ionescu E, Kleebe H-J, Riedel R. Strong influence of polymer architecture on the microstructural evolution of hafnium-alkoxide-modified silazanes upon ceramization. *Small* 2011;**7**(7):970–8.
5. Kleebe H-J, Gregori G, Weinmann M, Kroll P. Microstructure evolution and characterization. In: Colombo P, Riedel R, Sorarù GD, Kleebe H-J, editors. *Polymer derived ceramics: from nanostructure to applications*. Lancaster, PA, USA: DEStech Publications Inc.; 2009. p. 127–209.
6. Mera G, Riedel R, Poli F, Müller K. Carbon-rich SiCN ceramics derived from phenyl-containing poly(silylcarbodiimides). *J Eur Ceram Soc* 2009;**29**:2873–83.
7. Mera G, Tamayo A, Nguyen H, Sen S, Riedel R. Nanodomain structure of carbon-rich SiCN polymer-derived ceramics. *J Am Ceram Soc* 2010;**93**:1169–75.
8. Morcos RM, Mera G, Navrotsky A, Varga T, Riedel R, Poli F, Müller K. Enthalpy of formation of carbon-rich polymer-derived amorphous SiCN ceramics. *J Am Ceram Soc* 2008;**91**(10):3349–54.
9. Kleebe H-J, Gregori G, Babonneau F, Blum YD, MacQueen DB, Masse S. Evolution of C-rich SiOC ceramics. Part I. Characterization by integral spectroscopic techniques: solid state NMR and Raman spectroscopy. *Int J Mater Res* 2006;**97**(6):699–709.
10. Gregori G, Kleebe H-J, Blum YD, Babonneau F. Evolution of C-rich SiOC ceramics. Part II. Characterization by high lateral resolution techniques: electron energy loss spectroscopy. High-resolution TEM and energy filtered TEM. *Int J Mater Res* 2006;**97**(6):710–20.
11. Kleebe H-J, Blum YD. SiOC ceramic with high excess free carbon. *J Eur Ceram Soc* 2008;**28**:1037–42.
12. Martinez-Crespiera S, Ionescu E, Kleebe H-J, Riedel R. Pressureless synthesis of fully dense and crack-free SiOC bulk ceramics via photo-crosslinking and pyrolysis of a siloxane. *J Eur Ceram Soc* 2011;**31**(5):913–9.
13. Riedel R, Kienzle A, Dressler W, Ruwisch L, Bill J, Aldinger F. A silicoboron carbonitride ceramic stable to 2000 °C. *Nature* 1996;**382**:796–8.
14. Wang Z-C, Aldinger F, Riedel R. Novel silicon–boron–carbon–nitrogen materials thermally stable up to 2200 °C. *J Am Ceram Soc* 2001;**84**(10):2179–83.
15. Riedel R, Passing G, Schönfelder H, Brook RJ. Synthesis of dense silicon-based ceramics at low temperatures. *Nature* 1992;**355**:714–7.

16. Passing G, Schönfelder H, Riedel R, Brook RJ. Monolithic crack-free Si–C–N ceramic bodies derived from polysilazane forms. *Br Ceram Trans* 1993;**92**:21–2.
17. Seitz J, Bill J. Production of compact polysilazane-derived Si/C/N-ceramics by plastic forming. *J Mater Sci Lett* 1996;**15**:391–3.
18. Weinmann M, Haug R, Bill J, de Guire M, Aldinger F. Boron-modified polysilylcarbodiimides as precursors for Si–B–C–N ceramics: synthesis, plastic-forming and high-temperature behavior. *Appl Organomet Chem* 1998;**12**:725–34.
19. Haug R, Weinmann M, Bill J, Aldinger F. Plastic forming of preceramic polymers. *J Eur Ceram Soc* 1999;**19**:1–6.
20. Konetschny C, Galusek D, Reschke S, Fasel C, Riedel R. Dense silicon carbonitride ceramics by pyrolysis of cross-linked and warm pressed polysilazane powders. *J Eur Ceram Soc* 1999;**19**:2789–96.
21. Wan J, Gasch MJ, Mukherjee AK. Silicon carbonitride ceramics produced by pyrolysis of polymer ceramic precursor. *J Mater Res* 2000;**15**:1657–60.
22. Seitz J, Joachim B, Aldinger F, Naerheim Y. Process for Producing a Si/C/N Ceramic Body. US6458315, 2002, 6 p.
23. Shah SR, Raj R. Mechanical properties of a fully dense polymer derived ceramic made by a novel pressure casting process. *Acta Mater* 2002;**50**:4093–103.
24. Harshe R, Balan C, Riedel R. Amorphous Si(Al)OC ceramic from polysiloxane: bulk ceramic processing. Crystallization behavior and application. *J Eur Ceram Soc* 2004;**24**:3471–82.
25. Janakiraman N, Aldinger F. Fabrication and characterization of fully dense Si–C–N ceramics from a poly(ureamethylvinyl)silazane precursor. *J Eur Ceram Soc* 2009;**29**:163–73.
26. Jiang T, Hill A, Fei WF, Wei Y, Tellam M, Xu CY, An L. Making bulk ceramics from polymeric precursors. *J Am Ceram Soc* 2010;**93**(10):3017–9.
27. Su D, Li Y, An HJ, Liu X, Hou F, Li JY, Fu X. Pyrolytic transformation of liquid precursors to shaped bulk ceramics. *J Eur Ceram Soc* 2010;**30**:1503–11.
28. Vostokov IA, Dergunov YI, Gordetsov AS. Reaction of organosilicon, organogermanium, and organotin compounds with dicyanodiamide. New method for obtaining organoelemental carbodiimides. *Zh Obshch Khim* 1977;**47**:1769–71.
29. Shriver DF, Drezdzon MA. *The manipulation of air-sensitive compounds*. 2nd ed. New York: Wiley; 1986.
30. Ferrari AC, Robertson J. Interpretation of Raman spectra of disordered and amorphous carbon. *Phys Rev B* 2000;**61**:14095–107.
31. Ferrari AC, Meyer JC, Scardaci V, Casiraghi C, Lazzeri M, Mauri F, Piscanec S, Jiang D, Novoselov KS, Roth S, Geim AK. Raman spectrum of graphene and graphene layers. *Phys Chem Lett* 2006;**97**:187401-1–4.
32. Pimenta MA, Dresselhaus G, Dresselhaus MS, Cançado LG, Jorio A, Saito R. Studying disorder in graphite-based systems by Raman spectroscopy. *Phys Chem Chem Phys* 2007;**9**:1276–90.
33. Ferrari AC. Raman spectroscopy of graphene and graphite: disorder, electron–phonon coupling, doping and nonadiabatic effects. *Solid State Commun* 2007;**143**:47–57.
34. Cançado LG, Takai K, Enold E, Endo M, Kim YA, Mizusaki H, Jorio A, Coelho LN, Magalhaes-Paniago R, Pimenta MA. General equation for the determination of the crystallite size La of nanographite by Raman spectroscopy. *Appl Phys Lett* 2006;**88**:163106-1–3.
35. Sadezky A, Muckenhuber H, Grothe H, Niessner R, Pöschl U. Raman microspectroscopy of soot and related carbonaceous materials: spectral analysis and structural information. *Carbon* 2005;**43**:1731–42.
36. Zickler GA, Smarsly B, Gierlinger N, Peterlik H, Paris O. A reconsideration oft he relationship between the crystallite size L_a of carbons determined by X-ray diffraction and Raman spectroscopy. *Carbon* 2006;**44**:3239–46.
37. Saito R, Jorio a, Souza Filho AG, Dresselhaus G, Dresselhaus MS, Pimenta MA. Probing phonon dispersion relations of graphite by double resonance Raman scattering. *Phys Rev Lett* 2002;**88**:027401.
38. Lucchese MM, Stavale F, Martins Ferreira EH, Vilani C, Moutinho MVO, Capaz RB, Achete CA, Jorio A. Quantifying ion-induced defects and Raman relaxation length in graphene. *Carbon* 2010;**48**:1592–7.
39. Martins Ferreira EH, Moutinho MVO, Stavale F, Lucchese MM, Capaz RB, Achete CA, Jorio A. Evolution of the Raman spectra from single-, few, and many-layer graphene with increasing disorder. *Phys Rev B* 2010;**82**:125429-1–9.
40. Jorio A, Martins Ferreira EH, Cancado LG, Achete CA, Capaz RB. Measuring disorder in graphene with Raman spectroscopy. In: Mikhailov S, editor. *Physics and applications of graphene – experiments*. InTech; 2011. p. 439–54.
41. Kleebe H-J. Microstructure and stability of polymer-derived ceramics; the Si–C–N system. *Phys Status Solidi A* 1998;**166**:297–314.
42. Turquat C, Kleebe H-J, Gregori G, Walter S, Soraru GD. Transmission electron microscopy and electron-energy-loss spectroscopy study of nonstoichiometric silicon–carbon–oxygen glasses. *J Am Ceram Soc* 2001;**84**(10):2189–96.
43. Bréquel H, Parmentier J, Walter S, Badheka R, Trimmel G, Masse S, Latournerie J, Dempsey P, Turquat C, Desmartin-Chomel A, Le Neindre-Prum L, Jayasooriya UA, Hourlier D, Kleebe H-J, Sorarù GD, Enzo S, Babonneau F. Systematic structural characterisation of the high temperature behavior of nearly-stoichiometric silicon oxycarbide glasses. *Chem Mater* 2004;**16**(13):2585–98.
44. Tavakoli AH, Golczewski JA, Bill J. Decomposition and crystallization: thermal stability. In: Colombo P, Riedel R, Sorarù GD, Kleebe H-J, editors. *Polymer derived ceramics: from nanostructure to applications*. Lancaster, PA, USA: DEStech Publications Inc.; 2009. p. 211–30.
45. Tavakoli AH, Gerstel P, Golczewski JA, Bill J. Effect of boron on crystallization of amorphous Si–(B–)C–N polymer-derived ceramics. *J Non-Cryst Solids* 2009;**355**:2381–9.
46. Tavakoli AH, Golczewski JA, Bill J. Kinetic effect of boron on the thermal stability of Si–(B–)C–N polymer-derived ceramics. *Acta Mater* 2010;**58**:6002–11.
47. Janakiraman N, Weinmann M, Schuhmacher J, Müller K, Bill J, Aldinger F. Thermal stability. Phase evolution, and crystallization in Si–B–C–N ceramics derived from a polyborosilazane precursor. *J Am Ceram Soc* 2002;**85–87**:1807–14.
48. Janakiraman N, Zern A, Weinmann M, Aldinger F, Singh P. Phase evolution and crystallization in Si–B–C–N ceramics derived from a polyborosilazane precursor: microstructural characterization. *J Eur Ceram Soc* 2005;**25**:509–20.
49. Müller A, Gerstel P, Weinmann M, Bill J, Aldinger F. Correlation of boron content and high temperature stability in Si–B–C–N ceramics II. *J Eur Ceram Soc* 2001;**21**:2171–7.
50. Tavakoli AH. *Thermodynamic and kinetic studies on the thermal stability of amorphous Si–(B–)C–N ceramics*. PhD Thesis. Universität Stuttgart; 2010.
51. Gerstel P, Müller A, Bill J, Aldinger F. Synthesis and high-temperature behavior of Si/B/C/N precursor-derived ceramics without "Free Carbon". *Chem Mater* 2003;**15**:4980–6.
52. Wang Z, Gerstel P, Kaiser G, Bill J, Aldinger F. Synthesis of ultrahigh-temperature Si–B–C–N ceramic from polymeric waste gas. *J Am Ceram Soc* 2005;**88**:2709–12.